JACS
JOURNAL OF THE AMERICAN CHEMICAL SOCIETY
Article
pubs.acs.org/JACS

^{51}V NMR Crystallography of Vanadium Chloroperoxidase and Its Directed Evolution P395D/L241V/T343A Mutant: Protonation Environments of the Active Site

Rupal Gupta,[†] Guangjin Hou,[†] Rokus Renirie,[‡] Ron Wever,[‡] and Tatyana Polenova*[,†]

[†]Department of Chemistry and Biochemistry, University of Delaware, Newark, Delaware 19716, United States
[‡]Van't Hoff Institute for Molecular Science, University of Amsterdam, POSTBUS 94157, 1090 GD, Amsterdam, The Netherlands

Supporting Information

ABSTRACT: Vanadium-dependent haloperoxidases (VHPOs) perform two-electron oxidation of halides using hydrogen peroxide. Their mechanism, including the factors determining the substrate specificity and the pH-dependence of the catalytic rates, is poorly understood. The vanadate cofactor in the active site of VHPOs contains "spectroscopically silent" V(V), which does not change oxidation state during the reaction. We employed an NMR crystallography approach based on ^{51}V magic angle spinning NMR spectroscopy and Density Functional Theory, to gain insights into the structure and coordination environment of the cofactor in the resting state of vanadium-dependent chloroperoxidases (VCPO). The cofactor environments in the wild-type VCPO and its P395D/L241V/T343A mutant exhibiting 5−100-fold improved catalytic activity are examined at various pH values. Optimal sensitivity attained due to the fast MAS probe technologies enabled the assignment of the location and number of protons on the vanadate as a function of pH. The vanadate cofactor changes its protonation from quadruply protonated at pH 6.3 to triply protonated at pH 7.3 to doubly protonated at pH 8.3. In contrast, in the mutant, the vanadate protonation is the same at pH 5.0 and 8.3, and the cofactor is doubly protonated. This methodology to identify the distinct protonation environments of the cofactor, which are also pH-dependent, could help explain the different reactivities of the wild-type and mutant VCPO and their pH-dependence. This study demonstrates that ^{51}V-based NMR crystallography can be used to derive the detailed coordination environments of vanadium centers in large biological molecules.

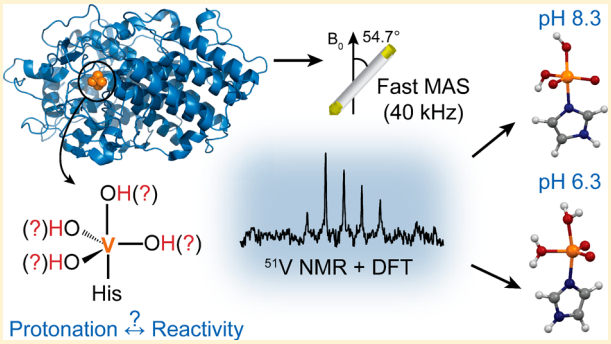

INTRODUCTION

Vanadium-dependent haloperoxidases (VHPOs) are a class of enzymes found both in marine and in terrestrial species, such as seaweeds, fungi, and lichens.[1] These enzymes are highly efficient catalysts for the two-electron oxidation of a halide ion in the presence of hydrogen peroxide, leading to the biosynthesis of halogenated natural products (Scheme 1).[2]

Scheme 1. Reaction Catalyzed by Vanadium-Dependent Haloperoxidases (VHPOs)[a]

$$H_2O_2 + H^+ + X^- \rightarrow H_2O + HOX$$

[a]X = Cl, Br, I.

VHPOs are named after the most electronegative halide they can oxidize; for example, vanadium chloroperoxidases (VCPOs) can oxidize Cl^-, Br^-, and I^-. VHPOs exhibit much higher turnover rates than any of the synthetic catalysts and have been attractive for applications in biotechnology.[1b,3] Consequently, understanding their catalytic mechanism is of interest to enable better design of robust synthetic halogenation catalysts for industrial applications.

Both synthetic chemists and biochemists have devoted efforts toward the elucidation of the enzymatic mechanism of VHPOs. For example, small inorganic complexes mimicking the peroxo-intermediate of VHPOs have been synthesized,[4] and laboratory-evolved mutants exhibiting significantly higher catalytic rates as compared to the wild-type enzyme have been developed, such as the P395D/L241V/T343A triple mutant of VCPO, which is a subject of this study.[5]

There are at least two major open questions concerning the enzymatic mechanism of VHPOs. One is what determines the substrate specificity, that is, whether a particular VHPO enzyme will be able to oxidize a chloride ion. Another is the pH-dependence of the catalytic activity as the reaction rates decreases significantly under basic conditions,[5,6] both in the wild type and in the P395D/L241V/T343A mutant of VCPO (Table 1). Curiously, the amino acids that undergo mutation in

Received: March 12, 2015
Published: April 9, 2015

ACS Publications © 2015 American Chemical Society

DOI: 10.1021/jacs.5b02635
J. Am. Chem. Soc. 2015, 137, 5618−5628

Table 1. Relative Catalytic Activity of Wild Type and the P395D/L241V/T343A Mutant VCPO[a]

	wild-type Br^- oxidation	P395D/L241V/T343A Br^- oxidation	wild-type Cl^- oxidation	P395D/L241V/T343A Cl^- oxidation
pH 8.0	1[b]	40,[b] 100[c]	N/D	N/D
pH 5.0	100[d]	575[d]	20[e]	36[e]

[a]Adapted from ref 5. [b]For 1 mM Br^-. [c]For 100 mM Br^-. [d]0.5 mM Br^-. [e]5 mM Cl^-.

the P395D/L241V/T343AVCPO mutant do not form direct hydrogen bonds with the vanadate cofactor (Figure 1), yet this

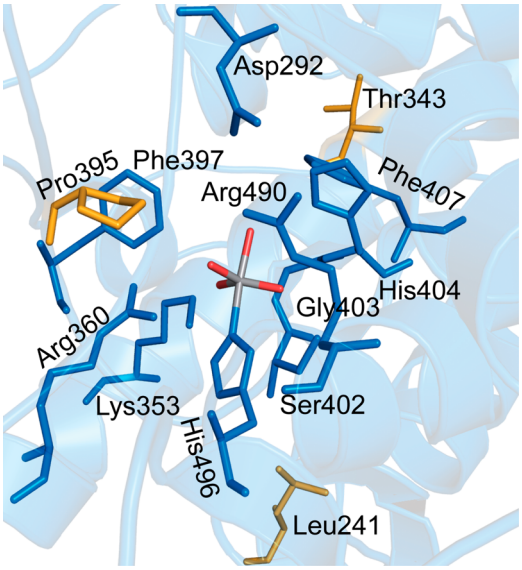

Figure 1. Active site geometry of VCPO from *C. inaequalis* (PDB code: 1IDQ) showing the key amino acid residues interacting with the vanadate cofactor. The residues colored gold are mutated in the P395D/L241V/T343A mutant.

triple substitution gives rise to a dramatically different catalytic profile vis-à-vis the wild type, with the rate enhancements for the bromination reaction of 100-fold at pH 8.0 and for the chlorination reaction of 36-fold at pH 5.0, respectively. The factors that dictate the catalytic rates of the wild type and the mutant are not fully understood. Answering these questions requires the knowledge of the detailed coordination environments of the vanadate cofactor and the amino acid residues in the active site, in the resting and peroxo forms of VHPOs, including their protonation states at different pH values. Such knowledge is currently lacking.

The X-ray structure of VCPO (a 67 kDa member of this family) from *C. inaequalis* at pH 8.0 has been solved at 2.1 Å resolution.[7] In addition, EXAFS measurements were performed on samples prepared at pH 6.0.[8] The X-ray structure revealed a vanadate cofactor bound directly to the His-496 residue of the polypeptide chain (Figure 1) and two crystallographic water molecules located above the vanadate cofactor.[7b] Furthermore, there are several other residues (e.g., K353, R360, R490, and H404) providing hydrogen bonds to the oxo groups. The vanadate center assumes trigonal bipyramidal geometry: three of the oxo-groups of vanadate lie on the equatorial plane, while the fourth oxygen is in the axial position, trans to the His-496 residue. At this resolution, the protonation state of the vanadate cofactor could not be unequivocally inferred from the structure. The refinement by the EXAFS data, however, suggests that one of the equatorial oxygens participates in a short V=O bond, both in the native and in the peroxo forms of the enzyme, indicating that the vanadate cofactor may have a distorted square pyramidal geometry.[8]

Several biochemical studies have shown that V(V) in the vanadate cofactor does not change its oxidation state during the catalysis,[8,9] as opposed to iron-based peroxidases where the oxidation state change on the metal is required for the completion of the reaction.[10] Therefore, we hypothesized that the protonation state of the oxo-groups of the vanadate ion could be responsible for redox tuning of the cofactor, further assisting in the catalysis. We posit that this may be partly responsible for the pH-dependent catalytic activity of these enzymes. The reaction cycle is known to go through an intermediate where the peroxide molecule binds to the vanadium center. This species, called the peroxo-intermediate, has been observed spectrophotometrically and by X-ray diffraction and XAS[7b,8,11] and by ^{51}V magic angle spinning (MAS) NMR in our laboratory.[12] Vanadium in its diamagnetic +5 oxidation state is spectroscopically silent, precluding its characterization with EPR. Employing UV−vis spectroscopy to monitor the changes in the vanadate cofactor is challenging due to lower extinction coefficients of the V^{+5} oxidation state,[11b] and site-specific assignments of the individual protons from UV−vis spectra are not readily attainable. The X-ray structure of the resting state and the peroxo-intermediate of VCPO[7b] has been seminal to our understanding of the geometry of the vanadate ion and the binding mode of the peroxide. However, the location of protons on the oxo groups or on the active site amino acids could not be resolved because of the limited resolution of these structures, nor could the structures be solved at different pH values, making it difficult to predict the protonation state changes with pH. Therefore, the reaction mechanism of these enzymes still awaits a complete characterization, leaving the questions of substrate specificity and pH-dependence of the catalytic rates open.

MAS NMR spectroscopy is an excellent tool to probe the diamagnetic vanadium center in VHPOs. ^{51}V is a spin-7/2 nucleus. It possesses a large gyromagnetic ratio, very high natural abundance (99.76%), and a relatively small nuclear quadrupole moment (-0.052×10^{-28} V/m^2), making it a sensitive NMR reporter. ^{51}V MAS NMR spectra yield information on the anisotropic quadrupolar and chemical shift interactions, which are exquisitely sensitive to the coordination environment of the metal center, as others and we have previously demonstrated.[13] Indeed, ^{51}V MAS NMR spectroscopy has been used to characterize a broad range of vanadium inorganic complexes in the past decade.[4,14] As we have demonstrated in multiple studies, ^{51}V NMR parameters are not only sensitive to the first coordination sphere, but they are also affected by the distal substituents,[14d,f] and to the presence of redox active ligands.[14k,l] ^{51}V MAS NMR can thus yield reliable information about the chemical nature of the vanadium center and the detailed ligand environments. This approach is particularly powerful when coupled with Density Functional Theory (DFT).[13,14g,h,15] NMR crystallography is another emerging technique that allows structural analysis of diamagnetic solids.[16] Recently, this approach was used to characterize oxovanadium(V) model complexes by multinuclear (^{51}V, ^{13}C, ^{15}N) MAS methods in conjunction with DFT.[17] In

DOI: 10.1021/jacs.5b02635
J. Am. Chem. Soc. 2015, 137, 5618−5628

Table 2. Experimental ^{51}V MAS NMR Parameters of the Wild Type and the P395D/L241V/T343A Mutant Vanadium Chloroperoxidase

	δ_{iso}[a] (ppm)	quadrupole-induced shift (ppm)	δ_σ (ppm)	η_σ	C_Q (MHz)	η_Q	α	β	γ
wild type pH 8.3	−520	11.9	−520 ± 15	0.4 ± 0.2	10.5 ± 1.5	0.5 ± 0.3	n.d.[b]	n.d.[b]	n.d.[b]
wild type pH 7.3	−520	11.9	−580 ± 20	0.4 ± 0.2	10.5 ± 1.5	0.5 ± 0.3	0	30	90
wild type pH 6.3	−420	29.3	−900 ± 25	0.5 ± 0.3	15.0 ± 1.5	0.9 ± 0.3	0	60	0
mutant pH 5.0	−526	21.7	−525 ± 25	0.5 ± 0.2	14.0 ± 1.0	0.6 ± 0.3	0	30	0
mutant pH 8.3 (second species)	−600	n.d.[b]	<−350	n.d.[b]	n.d.[b]	n.d.[b]	n.d.[b]	n.d.[b]	n.d.[b]

[a]Observed isotropic shift not corrected for the quadrupole-induced shift. [b]Cannot be determined.

this report, we employ ^{51}V-based NMR crystallography, for the first time, on a large biological molecule, to determine the protonation environment of the vanadate cofactor in vanadium-dependent chloroperoxidases.

In our early work, we have employed the combined MAS NMR and DFT approach to derive the protonation state and the coordination environment of the vanadate cofactor in the resting state of VCPO at pH 8.3.[18] Our results were independently supported by QM/MM calculations of large active site models.[19]However, at that time, the sensitivity of the NMR experiments was rather limited requiring huge amounts of protein (ca. 60−70 mg) and very long experiment times (5−7 days) to collect a single spectrum, precluding us from further investigating the different states of VCPO and its mutants. Because of these technical impediments, the active site coordination at pH values lower than 8.3, where the catalytic activity of the enzyme is optimal (pH 4.5−5.5), remains unknown. Furthermore, the origin of almost 100-fold higher bromination activity in the laboratory-evolved P395D/L241V/T343A mutant vis-à-vis the wild-type VCPO at pH 8 is not understood. This triple mutant also exhibits 100-fold and 5-fold higher bromination activity than the wild type at pH 8.0 and 5.0, respectively (Table 1).[5] It has been speculated that this improved activity is due to a change in the electron density on the oxygen atoms of the vanadate ion,[5] but further experimental evidence is needed to corroborate this hypothesis.

In this report, we have examined the coordination environment of the vanadium center in the wild type and P395D/L241V/T343A mutant VCPO, using ^{51}V MAS NMR and DFT calculations of extended active site models. The results reveal that the protonation states of the vanadate cofactor change as a function of pH, and that these protonation states are distinct for the wild-type enzyme and the mutant. On the basis of our findings, we propose a methodology that could help explain the large difference in the catalytic activities between the wild type and triple mutant VCPO and as a function of the pH. Broadly, the experimental approach presented here is applicable to detailed analysis of diamagnetic V(V) sites in a wide range of biological systems, including large proteins.

EXPERIMENTAL PROCEDURES

Protein Expression, Purification, and NMR Sample Preparation. The wild type and the P395D/L241V/T343A mutant VCPO enzymes were expressed in TOP10 *E. coli* host expression system and purified as reported previously.[5] MCD and phenol red assays were used to evaluate the activity of the enzymes, as described previously.[20] For vanadate incorporation, 80 mg/mL of protein in the appropriate buffer conditions (discussed below) was incubated overnight with 0.9 equiv of K_3VO_4 at 4 °C. This solution was frozen and lyophilized to generate NMR samples. 50 mM Tris-acetate buffer was used for samples prepared at pH 7.3, 8.3, and 9.0, while 50 mM MES buffer was used for protein samples generated at pH 6.3. In this article, the sample pH refers to the pH of the protein solution prior to lyophilization. This pH dictates the protonation of the vanadate cofactor. The lyophilization process is not expected to affect the protonation of the vanadate cofactor. When the lyophilized protein was tested using the MCD assay, full activity was observed, indicating that the lyophilization process did not affect the integrity of the active site of the enzyme.[18] The lyophilized VCPO also gave a positive phenol red assay test using the phenol red assay conditions that did not contain vanadate, also indicating that the integrity of the active site is preserved after lyophilization.

^{51}V MAS NMR Spectroscopy. ^{51}V MAS NMR spectra were acquired at 157.64 MHz (14.1 T) on a Varian InfinityPlus spectrometer equipped with a triple-resonance 1.6 mm Varian HXY probe. Another set of ^{51}V MAS NMR spectra was acquired at 20.0 T (^{51}V Larmor frequency of 223.58 MHz) on a Bruker Avance III spectrometer equipped witha 1.9 mm HX probe. The spectra for each sample were acquired at three MAS frequencies of 21, 31, and 40 kHz; the frequency was controlled to within ±10 Hz using the Varian or Bruker MAS controller. All spectra were acquired using a single-pulse excitation experiment with a pulse width of 0.7 μs at a B_1 field of 90 kHz; this is a nonselective pulse and excites both the central and the satellite transitions. We note that impurity signals from the rotor appear at 158.96 MHz (as confirmed by collecting the spectra of the empty rotor). The spectral width for the ^{51}V experiments was set at 2 MHz so that these signals did not overlap significantly with the protein signals and did not interfere with the spectral analysis. The spectra were processed in MestReNova using baseline correction and Gaussian apodization of 500−1000 Hz. Numerical simulations of the experimental ^{51}V MAS NMR spectra were performed using the SIMPSON software package.[21] For chemical shift parameter notation, we followed the Haeberlen−Mehring−Spiess convention,[22] where the three principal components of the CSA tensor, δ_{xx}, δ_{yy}, and δ_{zz}, and the isotropic component δ_{iso}, are defined according to $|\delta_{xx} - \delta_{iso}| \leq |\delta_{yy} - \delta_{iso}| \leq |\delta_{zz} - \delta_{iso}|$, and $\delta_{iso} = (\delta_{xx} + \delta_{yy} + \delta_{zz})/3$; the reduced anisotropy, $\delta_\sigma = \delta_{zz} - \delta_{iso}$; and the asymmetry parameter $\eta_\sigma = (\delta_{yy} - \delta_{xx})/(\delta_{zz} - \delta_{iso})$. The quadrupolar tensor is defined by the EFG tensor parameters as $C_Q = eQV_{ZZ}/h$ and $\eta_Q = (V_{YY} - V_{XX})/V_{ZZ}$, where $|V_{ZZ}| \geq |V_{YY}| \geq |V_{XX}|$ are the three components of the quadrupolar coupling tensor, e is the electronic charge, Q is the nuclear quadrupole moment, and h is Planck's constant. The parameters describing the quadrupolar and CSA tensors (δ_σ, η_σ, C_Q, η_Q) were determined by least-squares fitting of the simulated and experimental sideband intensities using a program written in Mathematica (Wolfram, Inc.) by one of the authors, as reported previously.[4,18a] The Euler angles (α, β, γ) describing the relative orientation of the CSA and the quadrupolar tensors were determined by visual comparison of the simulation and experimental sideband intensities. These best-fit NMR parameters and their corresponding error bars are reported in Table 2 for the various states of the wild type and the mutant enzyme studies in this Article.

Density Functional Theory Calculations. Density Functional Theory calculations were performed using the Gaussian09 software package for various models of the active site.[23] These models were generated using the vanadate cofactor and all surrounding amino acids and crystallographic water molecules within 5 Å from the cofactor in the crystal structure (PDB code: 1IDQ). The protonation state of the

DOI: 10.1021/jacs.5b02635
J. Am. Chem. Soc. 2015, 137, 5618−5628

Table 3. Protonation States of the VCPO Vanadate Cofactor Models Used in the DFT Calculations[a]

Model	δ_σ (ppm)	η_σ	C_Q (MHz)	η_Q	Experimental State
VOS4 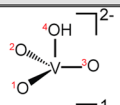	-443	0.67	7.0	0.69	N/A[b]
VOD14[c] 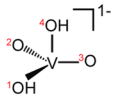	**-540**	**0.19**	**-7.5**	**0.4**	**Wild Type pH 8.3**
VOD24 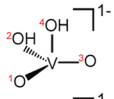	-357	0.18	-11.6	0.69	N/A
VOD34 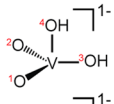	-400	0.89	-5.1	0.45	N/A
VOD44[c] 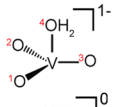	**-520**	**0.59**	**15.4**	**0.68**	**Mutant pH 5.0, 8.3**
VOT124 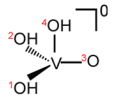	-250	0.69	-13.8	0.75	N/A
VOT134 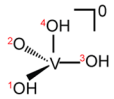	-359	0.65	10.7	0.34	N/A
VOT234[c] 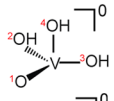	**-602**	**0.05**	**11.4**	**0.7**	**Wild Type pH 7.3**
VOT144 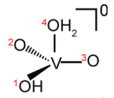	-736	0.42	12.8	0.84	N/A
VOT244[c] 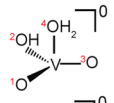	**-624**	**0.17**	**-11.4**	**0.74**	**Wild Type pH 7.3**
VOT344 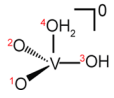	+482	0.37	-10.0	0.38	N/A

Model	δ_σ (ppm)	η_σ	C_Q (MHz)	η_Q	Experimental State
VOQ1244 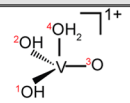	+652	0.25	-6.3	0.95	N/A
VOQ2344 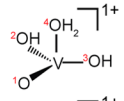	+892	0.45	-5.7	0.69	N/A
VOQ1144 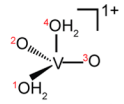	-771	0.8	21.9	0.66	N/A
VOQ2244[c] 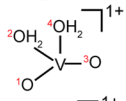	**-1034**	**0.68**	**15.8**	**0.46**	**Wild Type pH 6.3**
VOQ3344 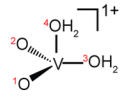	+509	0.77	-6.36	0.28	N/A

[a]The 3D structure and the Gaussian input files for eight extended active site models are shown in the Supporting Information. [b]Does not correlate to an experimentally observed state. [c]Highlighted in bold are the models that show agreement with the experimental values of δ_σ and C_Q.

vanadate cofactor was then manually changed to create input files for the individual models, and geometry optimization was performed on these starting structures. Sixteen different models were considered in this manner with quadruply, triply, and doubly protonated vanadate cofactor (see the Supporting Information for an example of one such input structure file; for other models, the coordination environments were the same except for the protons on the vanadate cofactor). For geometry optimizations, which were completed upon reaching the default convergence criterion, only the coordinates of all of the protons and the vanadate cofactor were allowed to change. NMR parameter calculation was performed by the GIAO method on the geometry-optimized structures using B3LYP hybrid functional and 6-311G(d,p) basis set. The nomenclature of these models is similar to that used by Waller et al.[19c] The oxygen atoms of the vanadate cofactor are labeled from 1 to 4 as reported in the crystal structure (Figure 6).[7b] VOQ refers to quadruply protonated vanadate, VOT refers to triply protonated vanadate, and VOD refers to a doubly protonated vanadate. The models under consideration are labeled after the oxygen atom protonated. For example, the triply protonated model that has an axial hydroxo group (on O^4) and oxygen 1 and 2 are protonated is labeled as VOT124. Similarly, the quadruply protonated model with axial water molecule and doubly protonated oxygen 1 is labeled as VOQ1144. Using the above nomenclature, the following models were computed using DFT: VOS4, VOD14, VOD24, VOD34, VOD44, VOT124, VOT134, VOT234, VOT144, VOT244, VOT344, VOQ1244, VOQ2344, VOQ1144, VOQ2244, VOQ3344. The NMR parameters computed from these models by DFT calculations are reported in Table 3. A comparison of experimental and DFT-predicted NMR parameters is provided in Table 4.

Table 4. Protonation States of the Active Site Vanadate Cofactor in Wild Type and P395D/L241V/T343A Mutant at Different pH Values: Summary of NMR Parameters Recorded Experimentally and Predicted by DFT

	δ_σ (ppm) experimental	δ_σ (ppm) DFT	C_Q (MHz) experimental	C_Q (MHz) DFT	DFT model
wild type pH 8.3	−520 ± 15	−540	10.5 ± 1.5	−7.5	VOD14
wild type pH 7.3	−580 ± 20	−624	10.5 ± 1.5	−11.4	VOT244
wild type pH 6.3	−900 ± 25	−1035	15 ± 1	15.4	VOQ2244
mutant pH 5.0	−525 ± 25	−520	14.0 ± 1.0	15.4	VOD44
mutant pH 8.3	−525 ± 25	−520	14.0 ± 1.0	15.4	VOD44

DOI: 10.1021/jacs.5b02635
J. Am. Chem. Soc. 2015, 137, 5618−5628

RESULTS

Optimal Sensitivity ^{51}V MAS NMR: Experimental Considerations. As described in the previous sections, our early studies of VHPOs by ^{51}V MAS NMR were impeded by limited sensitivity of the measurements. Another limitation was that VCPO had to be expressed in *Saccharomyces cerevisiae*, making incorporation of isotopic labels into the protein cost prohibitive.

To address the first challenge, we have turned our attention to fast-MAS probes featuring rotors of 1.6−1.9 mm size. As we have previously demonstrated in other contexts, these probes exhibit inherently higher sensitivity as compared to the probes outfitted with 3.2−5.0 mm rotors, and permitting work with small sample amounts.[24] For MAS NMR probes, reduced coil diameters provide enhanced sensitivity because rf efficiency is, to an approximation, inversely proportional to the square root of the coil volume.[25] However, this effect is in obvious contradiction to that SNR of an NMR experiment is approximately proportional to the sample volume.[26] The contemporary fast-MAS probes utilize rotor diameters of 0.7−1.9 mm and hence significantly reduced sample volumes. In the rotors whose diameters are 0.7−1.3 mm, sensitivity gains on a per unit mass of sample are realized, but the overall SNR is lower than that in the larger-diameter rotors. However, for fast-MAS probes with rotor diameters of 1.6−1.9 mm, a "sweet spot" is attained where the gain in sensitivity due to the reduced coil size outweighs the sensitivity losses due to reduced sample amounts. In practice, absolute sensitivity reached in these probes is higher despite smaller sample amounts. For example, in our studies of VCPO, when we packed the sample in a 3.2 mm rotor (ca. 15 mg of lyophilized protein), we had to add 100 000 transients to obtain a spectrum with sufficiently high SNR. In contrast, when we packed the sample into a 1.6 mm rotor (ca. 8 mg of lyophilized protein), a spectrum of similar SNR was instead acquired in approximately a quarter of the experiment time, with 28 000 transients added. No systematic investigation of the sensitivity of NMR experiments as a function of coil diameter for 1.3−4.0 mm rotors has been performed to our knowledge yet, but Nieuwkoop et al. have recently reported comparisons of the SNR for 1.3 and 1.9 mm rotors. Their studies indicate that, as compared to the 1.3 mm rotors, the 1.9 mm rotors exhibit up to 2.7 times improved sensitivity for 2D data acquisition and 5 times higher SNR for 1D ^{13}C direct detection.[27]

To resolve the second limitation, we have employed an *E. coli* expression system. The recombinant VCPO enzyme from *E. coli* was not characterized by NMR spectroscopy prior to this work. Similar to our prior study,[18] we assume that the active site of VCPO in the lyophilized state retains the same coordination environment and similar water content as in solution. This is a reasonable assumption because the NMR samples retained full enzymatic activity as monitored by the MCD and the phenol red assays (see Experimental Procedures).

Figure 2 depicts ^{51}V MAS NMR spectra of the wild-type VCPO purified from *E. coli* and prepared at pH 8.3. NMR spectra of the same enzyme purified from the *S. cerevisiae* were reported previously.[18a] NMR spectra of the protein purified from the two different expression systems are identical (see Supporting Information Figure S1), suggesting that the active site geometry does not change. We have additionally acquired ^{51}V MAS NMR spectra at the MAS frequency of 40 kHz. Under these conditions, the acquisition is much faster due to the improved sensitivity: the spectra could be acquired within 14 h using only 8 mg of VCPO. This is a tremendous gain in sensitivity when compared to our initial studies, where we had to use approximately 70 mg of protein and signal average for 5 days to obtain a single 1D spectrum. Figure 2 shows one such example ^{51}V MAS spectrum using a spinning frequency of 40 kHz acquired at the field strengths of 20.0 and 14.1 T together with the simulated spectra using the best-fit parameters from Table 2. These simulations show excellent agreement with the previously reported NMR parameters and indicate that (i) spectra acquired under the fast MAS conditions allow accurate determination of NMR parameters, and (ii) recombinant VCPOs prepared from *E. coli* and *S. cerevisiae* have identical vanadate cofactor structures, as expected.

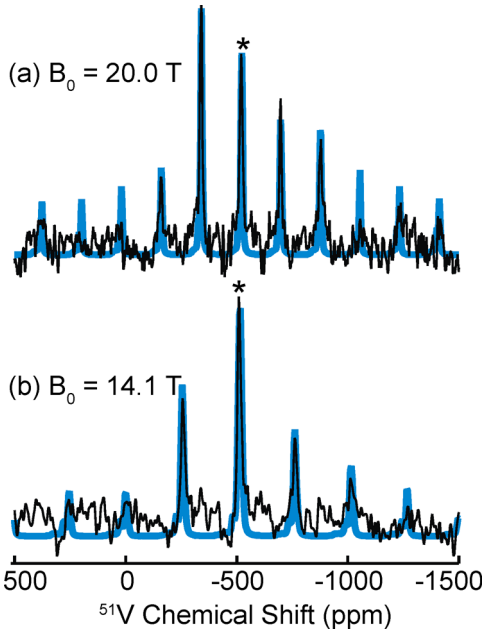

Figure 2. ^{51}V NMR spectra of wild-type VCPO at pH 8.3 acquired at the MAS frequency of 40 kHz and (a) B_0 = 20.0 T, (b) B_0 = 14.1 T. The experimental spectra are shown in black, while the simulated spectra are in blue. The isotropic chemical shift, δ_{iso} = −520 ppm, is marked with an asterisk. The simulations of the experimental spectra were performed in SIMPSON using the best-fit parameters as given in Table 2.

With the above improvements in the sample preparation and large sensitivity enhancements, we could proceed with the analysis of the structure of the vanadate cofactor in the resting state. As we demonstrate below, the use of fast-MAS probes and rotors with the diameter of 1.6−1.9 mm allows for efficient data acquisition at both fast and moderate spinning frequencies (40−20 kHz), enabling, for the first time, the characterization of the various states of VCPO. Specifically, we present the pH-dependence of the vanadate cofactor protonation states in the active site of the wild type and the P395D/L241V/T343A mutant of VCPO and discuss the role of these different states in the catalytic cycle.

Vanadate Cofactor in the P395D/L241V/T343A Mutant: ^{51}V MAS NMR at Different pH Values. *P395D/L241V/T343A Mutant at pH 5.0.* ^{51}V MAS NMR spectra for the P395D/L241V/T343Atriple mutant VCPO prepared at pH 5.0, recorded at the MAS frequencies of 21, 31, and 40 kHz, are shown in Figure 3 (left panel). The observed isotropic chemical

DOI: 10.1021/jacs.5b02635
J. Am. Chem. Soc. 2015, 137, 5618−5628

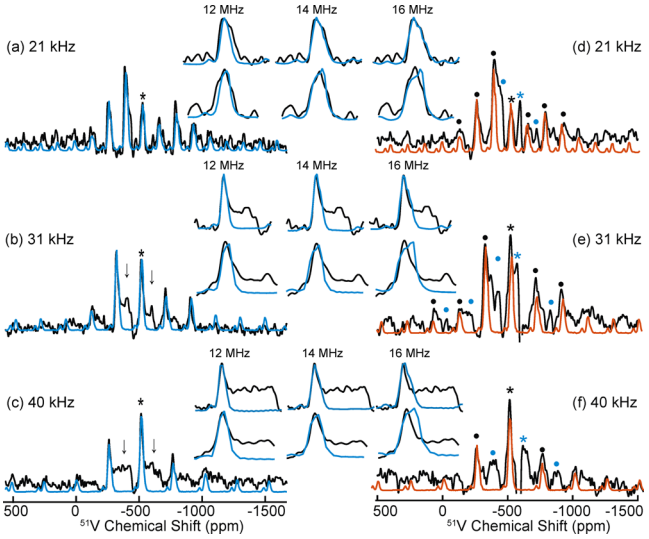

Figure 3. Left: 14.1 T ^{51}V MAS spectra of P395D/L241V/T343A mutant VCPO at pH 5.0 acquired with MAS frequencies of (a) 21 kHz, (b) 31 kHz, and (c) 40 kHz. The experimental spectra are shown in black, while the simulated spectra are in blue. The isotropic chemical shift is marked with an asterisk. The simulations of the experimental spectra were performed in SIMPSON using the best-fit parameters given in Table 2. The broad features marked with arrows in the spectra acquired at 31 and 40 kHz belong to minority species, which are not visible at slower MAS frequencies. An expansion showing the far left highest-intensity spinning sideband and the isotropic spinning sideband with simulated spectra overlaid on top for C_Q = 14 MHz, which gives the best fit to the experimental data (middle), C_Q = 12 MHz (left) and C_Q = 16 MHz (right) shown as inset. All other NMR parameters for simulations were kept the same as in Table 2. Right: 14.1 T ^{51}V MAS spectra of P395D/L241V/T343A mutant VCPO at pH 8.3 acquired at the MAS frequencies of (d) 21 kHz, (e) 31 kHz, and (f) 40 kHz. The signals from the species similar to that of pH 5.0 are marked in black with the spinning sidebands labeled as dots and the isotropic chemical shift labeled with an asterisk. Similarly, the signals associated with the second species observed at pH 8.3 are marked in blue. The brown traces are the simulations for the major species present at pH 8.3 overlaid on top of the experimental data.

shift is −526 ppm, 6 ppm upfield as compared to the wild-type enzyme at pH 8.3 (δ_{iso} = −520 ppm). The dominant spinning sidebands originate from the central transition. The overall spectral envelope suggests that the reduced anisotropy, δ_σ = −525 ± 25 ppm, is very similar to the wild-type enzyme at pH 8.3 (Figure 2).

The line widths of the individual spinning sidebands are larger as compared to those of the wild-type enzyme at pH 8.3 shown in Figure 2. The increase in the line widths could be due to the following: (i) multiple conformations in the powder sample, or (ii) broadening due to the increase in the magnitude of the second-order quadrupolar interaction. Because both the wild type and the P395D/L241V/T343A mutant samples were prepared using the same procedure, it is unlikely that the sample preparation protocol caused the variation in the line widths. On the other hand, as described in our previous work, the second-order ^{51}V quadrupolar interaction, which is not averaged by MAS, introduces line broadening and line shifts, and these can be explicitly predicted by numerical simulations.[18a] Therefore, we hypothesized that the increased line widths for the P395D/L241V/T343A mutant are suggestive of a larger magnitude of C_Q, vis-à-vis the wild-type VCPO at pH 8.3.

Figure 3 shows the experimental and the simulated spectra for the MAS frequencies of 21, 31, and 40 kHz. All of the simulations were performed using the same best-fit parameters shown in Table 2. The insets in Figure 3 (left panel) show an expansion around one of the central-transition peaks at the MAS frequencies of 21, 31, and 40 kHz with simulations for C_Q = 12, 14, and 16 MHz overlaid on top. All of the simulations in these insets were generated using the same NMR parameters except for C_Q. It is noteworthy that a C_Q = 14 MHz predicts the line shape reasonably well, while C_Q values of 12 MHz or lower render the line widths that are narrower than the experimental data. Similarly, C_Q of 15.5 MHz or larger gives rise to line widths broader than those in the experimental data. This result suggests that C_Q is in the range of 14 ± 1 MHz. The broad features present in the experimental data acquired with spinning frequencies of 31 and 40 kHz are due to the presence of a minority species (marked with arrows in Figure 3, left panel). As discussed below, the concentration of this species increases as the pH of the sample is raised.

P395D/L241V/T343A Mutant at pH 8.3. Figure 3 (right panel) shows ^{51}V MAS NMR spectra of the P395D/L241V/T343A mutant prepared at pH 8.3 recorded at the MAS frequencies of 21, 31, and 40 kHz. Despite the fact that these spectra are remarkably similar to those of the sample prepared at pH 5.0, there is clear evidence of the presence of a second species that coexists with the major species. Spinning sidebands separated by the MAS frequency can be easily detected in spectra acquired with ν_r = 21 kHz, for two chemically different ^{51}V environments. For the MAS spectra recorded at 31 and 40 kHz, the spinning sidebands can be detected but have broad line widths (Figure 3d and e). The detection of multiple spinning sidebands from the second species suggests that it has a measurable chemical shift anisotropy. The isotropic chemical shift of this species is approximately −600 ppm, which is significantly different from that of the wild type at near neutral pH, as well as from that of the mutant sample prepared under acidic conditions. A difference spectrum generated by subtracting the major mutant species at pH 5.0 does not have sufficiently high SNR. The simulations of the difference spectrum indicate a relatively small CSA tensor (<−350 ppm), but the quadrupolar coupling constant cannot be determined. Quantitation of the amount of the minor species is not trivial because its quadrupolar and chemical shift parameters determining the overall width of the central transition as well as the line widths of the individual spinning sidebands differ significantly from those for the major species. However, a rough estimate based on the line widths and peak intensities indicates that at pH 5.0, this species could account for 10−20% of vanadate, while at pH 8.3, approximately 40% of vanadate could be present in this form.

Therefore, the P395D/L241V/T343A mutant at pH 8.3 shows the presence of two species: the same major species as that observed at pH 5.0, and a second, minor, species with significantly different CSA and isotropic chemical shift. The origin of this second species is not clear in the present studies, and a more detailed investigation will be performed in the future to elucidate the nature of this speciation.

Vanadate Cofactor in the Wild-Type VCPO: pH-Dependence of the ^{51}V MAS NMR Spectra. The NMR spectra of VCPO prepared at pH 8.3 and 9.0 are identical. Upon a cursory look, the NMR spectra of the VCPO samples

DOI: 10.1021/jacs.5b02635
J. Am. Chem. Soc. 2015, 137, 5618−5628

prepared at pH 7.3, 8.3, and 9.0 are also similar. However, as shown in Figure 4a and c, the simulations performed using the

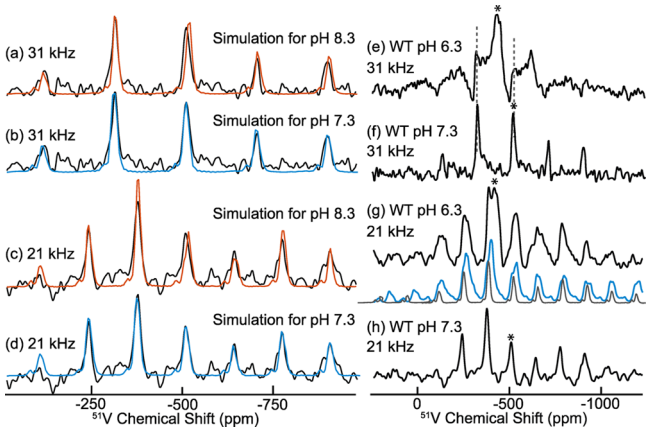

Figure 4. Left: 14.1 T ^{51}V MAS NMR spectra of wild-type VCPO prepared at pH 6.3 and 7.3. Left: The experimental spectra (black) for VCPO at pH 7.3 were acquired at the MAS frequencies of 21 and 31 kHz with simulations overlaid on top (brown and blue). The simulated data in (a) and (c) used the same parameters as those for the enzyme at pH 8.3 (brown traces); note considerable deviations between the intensities, frequencies, and line widths of the experimental and simulated sidebands. The simulated data in (b) and (d) used the best-fit parameters reported in Table 2; note excellent agreement between the intensities, frequencies, and line widths of the experimental and simulated sidebands. At pH 8.3, δ_σ = −520 ppm, whereas at pH 7.3, δ_σ = −580 ppm (blue traces). Right: A comparison of NMR spectra of the wild-type VCPO at pH 6.3 (e and g) and 7.3 (f and h). Simulations of the two species present at pH 6.3 are shown as blue (major species) and gray (minor species similar to that at wild type pH 7.3) traces for ν_r = 21 kHz. The isotropic chemical shift is labeled with an asterisk. As discussed in the text, these differences reflect the changes in the protonation state of the vanadate cofactor at the three pH values.

best-fit parameters obtained for the sample at pH 8.3 do not correctly predict the line shape and the intensities of the spinning sidebands for the spectra recorded at pH 7.3. To recapitulate these spectra, a larger CSA is required, δ_σ = −580 ± 20 ppm (as compared to −520 ppm for samples prepared at pH 8.3 and 9.0). Furthermore, the Euler angles describing the relative orientations of the quadrupolar and CSA tensors are different in the two sets of spectra: for those at pH 7.3, (α, β, γ) = (0, 30, 90). The isotropic peak and the quadrupolar tensor parameters remain the same for all three pH values.

At pH 6.3, the 31 kHz MAS NMR spectrum of the wild type clearly indicates the presence of two species: a minority species identical to that formed at pH 7.3 (shown by dashed lines in Figure 4e and f), and a majority species that has broader line widths as compared to that of the samples at higher pH. The presence of two species is less apparent at ν_r = 21 kHz because the spinning side bands of the two species overlap. Note that at this pH, an increase in the magnitude of the quadrupolar interaction for the major species is manifested in the broadening of the individual spinning sidebands as observed in the case of the P395D/L241V/T343A mutant. The isotropic chemical shift for the majority species is −420 ppm as compared to the isotropic shift of −520 ppm for the protein prepared at pH 7.3−9.0. Numerical simulations of this species (Table 2) reveal dramatically different NMR parameters for this state of the enzyme as compared to the environments at higher pH: δ_σ = −900 ± 25 ppm, C_Q = 15 ± 1.5 MHz, and (α, β, γ) = (0, 60, 0). At 21 kHz MAS, a simulation comprised of the major species and the minor species similar to wild type at pH 7.3 is needed to recapitulate the experimental spectrum (Figure 4, right panel). These differences in NMR parameters are indicative of a change in the coordination environment of the vanadate cofactor as the pH is altered.

DISCUSSION

Comparison of Wild Type and the P395D/L241V/T343A Mutant ^{51}V NMR Spectra. Figure 5 shows a comparison of the ^{51}V MAS NMR spectra of the wild-type VCPO (prepared at pH 6.3 and 8.3) and the P395D/L241V/T343A mutant VCPO (prepared at pH 5.0 and 8.3). It is clear from the figure that the spectra associated with each sample exhibit significant differences. The wild-type VCPO at pH 8.3 and the P395D/L241V/T343A mutant at pH 5.0 have similar chemical shift anisotropy but very different quadrupolar coupling constants. At the MAS frequency of 21 kHz, the P395D/L241V/T343A mutant at pH 8.3 clearly shows the evidence of two species, while the presence of two species is not as obvious for the sample prepared at pH 5.0 with the current signal-to-noise ratio (Figure 5). At higher MAS frequencies (31 and 40 kHz, Supporting Information Figure S2), weak spinning sidebands originating from the minority species can be observed for the sample prepared at pH 5.0. Similarly, the presence of minority species is clearly evident in the spectrum of the wild type at pH 6.3 acquired at ν_r = 31 kHz; however, when ν_r = 21 kHz, the spinning sidebands of the two species overlap, making their detection difficult. These findings further exemplify the advantages of using fast MAS frequencies (40 kHz or greater) for investigation of low-sensitivity systems including determination of minor species. Fast MAS frequencies are also beneficial in the determination of relative orientation of the CSA and the quadrupolar tensors, which was not possible in our previous studies of VCPO conducted at moderate MAS frequencies (see the Supporting Information for an additional discussion).

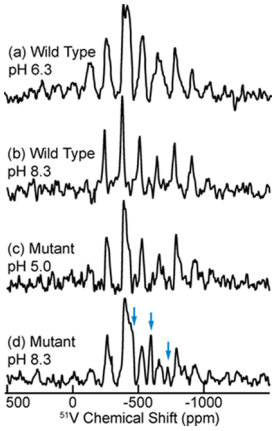

Figure 5. ^{51}V MAS NMR spectra of VCPO and its mutant at 14.1 T and ν_r = 21 kHz: (a) wild-type enzyme at pH 6.3; (b) wild-type enzyme at pH 8.3; (c) P395D/L241V/T343A mutant at pH 5.0; and (d) P395D/L241V/T343A mutant at pH 8.3. The arrows indicate the spinning sidebands associated with the second species in the P395D/L241V/T343A mutant.

Active Site Coordination Environments in VCPO: General Considerations. The protonation state of the vanadate cofactor is critical to our understanding of the

DOI: 10.1021/jacs.5b02635
J. Am. Chem. Soc. 2015, 137, 5618−5628

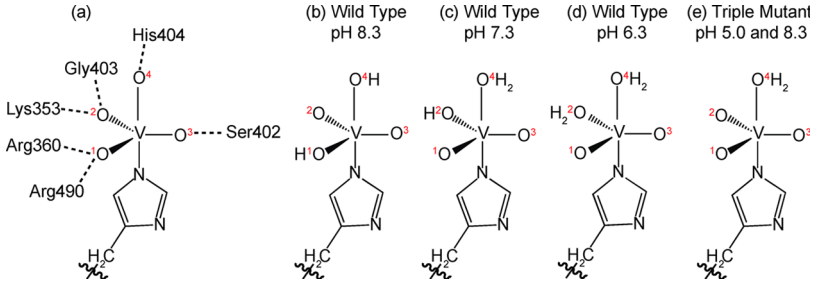

Figure 6. Hydrogen bonding and the proposed protonation states of the vanadate cofactor for the wild type and the mutant enzyme at the various pH values studied in this report. (a) Hydrogen-bonding interactions for the vanadate cofactor with the amino acids in the active site as observed in the X-ray structure of VCPO (PDB code: 1IDQ). (b–d) The protonation states of vanadate cofactor in the different VCPO samples derived from the combined ^{51}V MAS NMR and DFT approach: wild-type VCPO at pH 8.3 (b); wild-type VCPO at pH 7.3 (c); wild-type VCPO at pH 6.3 (d); and the major species of P395D/L241V/T343A mutant at pH 5.0 and 8.3 (e).

catalytic mechanism of VHPOs. During the catalytic cycle, the vanadium(V) center does not change its oxidation state, leaving the variations in the protonation states of the oxo groups as one of the mechanisms that could control the redox potential at different pH values and allowing the reaction to proceed. Thus, the knowledge of protonation state of the vanadate cofactor is important for the elucidation of the pH-dependent catalytic activity of VCPO.

The determination of the protonation state of the oxo groups is particularly challenging because the position of the protons cannot be located in the crystal structure with available resolution. As demonstrated in our early work, ^{51}V MAS NMR is uniquely suited for deriving the protonation states in VCPO.[18a] In that study of the wild-type VCPO at pH 8.3, we discovered that the vanadate cofactor is doubly protonated, in agreement with the QM/MM predictions and in contrast to the singly protonated state postulated from the limited-resolution X-ray structure. In this work, we have addressed the pH-dependence of the protonation states of the vanadate cofactor in the wild type and P395D/L241V/T343A mutant VCPO. This has become possible due to the major technical improvements, availability of fast MAS probes, rendering dramatic sensitivity enhancements and at the same time permitting measurements with small sample amounts.

A number of experimental values for the isotropic chemical shifts of ^{51}V nuclei in various vanadium containing polypeptides have been reported,[18a,28] and most of these are found to be in the range of −507 to −542 ppm. In addition, extensive quantum mechanics/molecular mechanics (QM/MM) calculations performed by Waller et al. also gave a similar range for the isotropic chemical shifts for various protonation states of vanadate cofactor.[19c] This suggests that isotropic chemical shifts alone cannot be used as an indicator for the protonation state. On the other hand, the anisotropic NMR parameters, CSA, and quadrupolar tensor components as well as their relative orientations, obtained from ^{51}V MAS NMR parameters, are exquisitely sensitive to the protonation states. Furthermore, as we have demonstrated, a combined ^{51}V MAS and computational approach allows for the determination of the active site coordination of VCPO.[18a] Waller et al. calculated NMR parameters at the QM/MM level for various large models of the VCPO active site and then correlated their findings to the experimental parameters from MAS NMR measurements reported by us.[19c] A different approach was used by Zampella et al.[19a] and by us, in which gas-phase DFT calculations were performed on a series of smaller active site models to obtain the states corresponding to the energetic minima and correlate those to the various experimental measurements. Bangesh et al. performed TD-DFT calculations on imidazole bound vanadate models, and Raugei et al. pursued a QM/MM study.[29] Interestingly, all of these approaches came to a similar conclusion, where an anionic cofactor with two hydroxo groups and two oxo groups was considered as the most likely resting state. Zhang et al. concluded that the resting state is more like a doubly protonated vanadate cofactor with an axial water molecule, using QM/MM calculations.[30] Nevertheless, the exact position of the protons, that is, whether both are in the equatorial plane and which of the three oxo groups are protonated, still remained unclear.

A major drawback in using small active site models for DFT calculations is that they do not account for the salient H-bonding interactions with the amino acid residues that play a key role in defining the protonation state of the vanadate and the catalysis by VCPO. The previously reported calculations on large QM/MM models of the active site did consider H-bonding; however, at the time of their publication, there were no experimental ^{51}V MAS NMR results available at neutral or acidic pH's, and hence assignment of the corresponding protonation states could not be made.[19c] In this work, we have performed DFT calculations on large active site models from the crystal structure that consider the key hydrogen bonds to the cofactor. The coordinates of the heavy atoms (C, N, and O) were not allowed to change, and geometry optimization was performed on the protons and the vanadate cofactor. Figure 6a shows the H-bonds between the four vanadate oxo-groups and the protein polypeptide chain as observed in the X-ray structure.[7a] Because of the inherent uncertainties in the calculation and the experimental data, for the following discussion, we will consider the trends in the predicted CSA and C_Q, rather than the absolute values, to make correlations with the experimental data.

Wild Type and P395D/L241V/T343A Mutant VCPO: pH-Dependence of the Vanadate Cofactor's Protonation States and Implications for the Catalytic Mechanism. DFT and QM/MM calculations on active site models of different size have proposed a doubly protonated vanadate cofactor where two of the oxygen atoms are protonated to hydroxo groups. One of the hydroxo groups is axial to the His-496 residue, while the exact location of the second hydroxo group that is believed to be in the equatorial plane is not clear. In their QM/MM studies, Waller et al. ruled out the possibility of O^2 being protonated upon visual observation of the lack of H-bond acceptors in the nearby amino acids.[19c] The DFT calculations presented in this study also suggest a doubly

DOI: 10.1021/jacs.5b02635
J. Am. Chem. Soc. 2015, 137, 5618–5628

protonated vanadate cofactor, in agreement with previous reports.[18a,19a,29a] Table 3 provides the computed NMR parameters for all models considered in this report. NMR parameters predicted by the model VOD14 (δ_σ^{DFT} = −540 ppm and C_Q^{DFT} = −7.5 MHz, Table 4) agree with the experimental data for the wild-type enzyme at pH 8.3. It is noteworthy that, although the DFT calculations give the sign of the quadrupolar coupling, the experimental spectra only depend on the magnitude of C_Q. The calculations also rule out the possibilities for the VOD24 and VOD34 models, as the NMR parameters from these models did not agree with experimental results. Importantly, these results not only strongly indicate that vanadate cofactor at pH 8.3 is doubly protonated with an axial and an equatorial hydroxo group, but also suggest that protonated oxygen in the equatorial plane is the one that forms H-bonds with Arg-360 and Arg-490 (O^1, Figure 6b). The protonation state of the resting cofactor could have direct implications on the formation of the peroxo-intermediate, as will be discussed later.

Two triply protonated models gave parameters that agree reasonably well with the experimental results for the wild-type enzyme at pH 7.3: VOT234 (δ_σ = −602 ppm and C_Q = 11.4 MHz, Table 3) and VOT244 (δ_σ^{DFT} = −624 ppm and C_Q^{DFT} = −11.4 MHz, Table 3). As the pH is lowered to 7.3, the experimental value of δ_σ increases to −580 ppm but the magnitude of C_Q remains the same. For this pH, the most likely state is a triply protonated model in which the axial oxygen, O^4, is water and O^2 is protonated to hydroxo group (VOT244, Table 4 and Figure 6c). This model is most reasonable as an axial water molecule will favor the dissociative mechanism in which the axial oxygen molecule gets dissociated from the vanadate cofactor, allowing the peroxide to bind (Scheme 2).[31]

Scheme 2. A Schematic Representation of the VCPO Reaction Cycle under Dissociative Pathway[a]

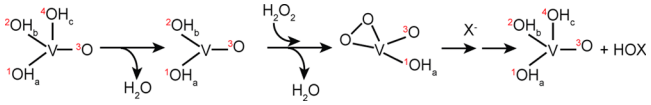

[a]The subscript on H represents the number of protons on the respective oxo group: *a* = 1 for the wild type at pH 8.3 and 0 for all other pH values for the wild type and mutant; *b* = 0 for the wild type at pH 8.3 and mutant, 1 for the wild type at pH 7.3, and 2 for wild type at pH 6.3; and *c* = 1 for the wild-type enzyme at pH 8.3 and 2 for all other pH values of the wild type and the mutant studied in this Article.

A weaker axial V−OH_2 bond (at pH 7.3) will undergo dissociation with relatively more ease as compared to a V−OH bond (at pH 8.3), consequently improving the catalytic efficiency (Scheme 2). This suggests that as the pH is lowered from 8.3 to 7.3, a protonation step takes place, and the axial group of the vanadate cofactor changes from hydroxo to water (Figure 6c). This protonation step also changes the overall charge of the vanadate cofactor from anionic to neutral. It is noteworthy that even though our results suggest that the axial oxo group gets protonated as the pH is lowered, which may energetically favor peroxide binding, UV−vis studies suggest that its binding efficiency improves as the pH in increased,[11b] suggesting that the steps following the peroxide binding also play a prominent role in the pH-dependent catalytic activity of this class of enzymes.

The significant increase in the magnitudes of C_Q and δ_σ for the wild-type enzyme at pH 6.3 can be predicted by a quadruply protonated model, VOQ2244 (δ_σ^{DFT} = −1035 ppm and C_Q^{DFT} = 15.4 MHz, Table 4 and Figure 6d), suggesting that lowering pH from 7.3 to 6.3 results in another protonation event at equatorial oxygen O^2. The vanadate cofactor in this state of the enzyme has a positive charge of +1. As mentioned above, the presence of water ligands could presumably improve peroxide binding during the catalytic cycle.

The P395D/L241V/T343A mutant at pH 5.0 exhibits a very similar CSA tensor to that of the wild-type enzyme at pH 8.3 (δ_σ = −520 ppm) but a larger C_Q of 14 MHz (as compared to 10.5 MHz for the wild-type enzyme). This state represents the major species both at pH 5.0 and 8.3 for the mutant enzyme. X-ray structures of the apo VCPO and its five active mutants showed no changes in their secondary structure. This suggests that the P395D/L241V/T343A mutations should not significantly alter the rigid secondary structure of the enzyme.[2b] The only model that yielded parameters in agreement with the experimental results is the doubly protonated vanadate with an axial water group, VOD44 (δ_σ^{DFT} = −520 ppm and C_Q^{DFT} = 15.4 MHz, Table 4). This model (Figure 6e) is different from the wild-type active site as in the latter O^1 is protonated. It is noteworthy that even though the mutations performed in the P395D/L241V/T343A mutant do not alter the direct hydrogen-bonding network of the vanadate cofactor, the differences in the NMR parameters indicate a nontrivial change in the electron density around the vanadium center. We speculate that these three amino acid substitutions at the distal sites perturb the entire hydrogen-bonding network including changes for the amino acids in the immediate vicinity of the vanadate cofactor. In the future, we will employ MAS NMR to get information on the hydrogen-bonding environments in VCPO, by recording ^1H, ^{13}C, and ^{15}N CSA tensors for the individual amino acid residues. Interestingly, Hasan et al.[5] proposed that the increased activity of the mutant could be due to the introduction of negative charge by the P395D mutation, which would in turn affect the charge on O^1. Therefore, the model that we derive on the basis of our current results with changes in the protonation state of O^1 for the wild type at pH 8.3 and the P395D/L241V/T343A mutant is in consensus with this hypothesis whereby the P395D mutation facilitates negative charge on O^1. The large quadrupolar coupling constant for the P395D/L241V/T343A mutant (14 MHz) as compared to the wild-type enzyme at pH 7.3−9.0 (10.5 MHz) indicates a significant change in the charge distribution of the vanadium center. Deprotonation of O^1 and conversion of axial hydroxo to aqua group give rise to such change in the quadrupolar coupling constant, as indicated by the DFT calculations.

The minority species that is present in the samples of the P395D/L241V/T343A mutant VCPO and whose concentration decreases with the decrease of the pH has significantly lower reduced anisotropy (δ_σ < −350 ppm), and the C_Q for this species could not be determined due to the relatively low signal-to-noise ratio of the corresponding peaks in the experimental data. The triply protonated models that predict similar CSA parameters are the states where oxygens 1, 3, and 4, or 2, 3, and 4 are protonated. In addition to this, doubly protonated models where either O^1 or O^3 is protonated together with an axial hydroxo group (O^4) can also be considered. However, due to the lack of information about the quadrupolar tensor, none of the above models can be preferred over others. It is worth mentioning that the biological origin of this second species is not clear from the current studies, but because this is a minority species, it is unlikely to contribute to

DOI: 10.1021/jacs.5b02635
J. Am. Chem. Soc. 2015, 137, 5618−5628

the 100-fold improved catalytic efficiency of the mutant at pH 8. Therefore, the resting state associated with the major species of the vanadate cofactor in the P395D/L241V/T343A mutant is likely to be the same at both pH 5.0 and 8.3, and presumably the steps downstream the reaction path, following the peroxide binding, dictate the differences in catalytic activity as a function of pH for the mutant. Although unlikely, the role of the minority species in the catalytic rates of the mutant cannot be completely ruled out on the basis of the results from this study, and additional experiments are underway to elucidate the nature and origin of these species.

Taken together, these studies indicate that even though the catalytic activity of VCPO depends highly on pH, the vanadate cofactor's resting state and its protonation are only partially responsible for this dependence. However, the steps following peroxide binding are expected to also play a very important role in tuning the catalytic profile of haloperoxidases. A DFT study on small model complexes by Zampella et al. suggests that the protonation of the peroxo intermediate could play an important role in the catalytic cycle.[32] Specifically, on the basis of this work, it was concluded that, for the crucial oxo transfer (to the substrate) step to take place in the reaction cycle, the pseudoaxial oxygen atom of the peroxo intermediate must be deprotonated and should not be involved in any hydrogen-bonding interactions. These DFT studies of the reaction intermediates are in consensus with the results presented in this report, suggesting that the protonation state of the reaction intermediates may play a key role in the catalytic profile of these enzymes. Therefore, studying various intermediates along the reaction path, including the peroxo-intermediate, with hybrid MAS NMR/DFT approach will be important for complete understanding of the reaction mechanism, including pH-dependence and substrate specificity, for this class of enzymes.

CONCLUSIONS

By an integrated ^{51}V MAS NMR and DFT, we have derived the protonation states of vanadate cofactor in the resting state of the wild type and P395D/L241V/T343A mutant of vanadium chloroperoxidase. The large sensitivity enhancements attained in the current study due to the fast MAS probe technology enabled the assignment of the location and number of protons on the vanadate cofactor for the first time. In the wild-type VCPO, the vanadate cofactor at pH 8.3 is doubly protonated with axial hydroxo group, triply protonated with anaxial water molecule at pH 7.3, and quadruply protonated with axial and equatorial water molecules at pH 6.3. The NMR parameters of the P395D/L241V/T343A mutant are indicative of a doubly protonated cofactor with an axial water molecule. This assignment of the location and number of protons on the vanadate cofactor gives insight into the structural differences in the active site of the wild type and the mutant enzyme as a function of pH. The experimental protocols established in this work will enable analysis of resting and peroxo intermediate states of the vanadate cofactor in the various vanadium haloperoxidases, which is anticipated to resolve the current controversies concerning their catalytic mechanisms. Finally, the approach presented here is broadly applicable for the investigations into geometric and electronic structure of diamagnetic vanadium sites in dilute environments, including but not limited to vanadium-containing biomacromolecules.

ASSOCIATED CONTENT

Supporting Information

Comparison of wild-type (pH 8.3) and mutant (pH 5.0 and 8.3) MAS NMR data at 21, 31, and 40 kHz MAS, spectra of the wild-type enzyme from *E. coli* and *S. cerevisiae*, a discussion on the determination of relative orientation of the CSA and quadrupolar tensors using fast MAS, and the coordinates of the structure used for DFT calculations. This material is available free of charge via the Internet at http://pubs.acs.org.

AUTHOR INFORMATION

Corresponding Author

*tpolenov@udel.edu

Notes

The authors declare no competing financial interest.

ACKNOWLEDGMENTS

This work was supported by the US-Israel Binational Science Foundation (Grant 2011077). We acknowledge the support of the National Science Foundation (NSF Grant CHE0959496) for the acquisition of the 850 MHz NMR spectrometer at the University of Delaware and of the National Institutes of Health (NIH Grants P30GM103519 and P30GM110758) for the support of core instrumentation infrastructure at the University of Delaware.

REFERENCES

(1) (a) Vollenbroek, E. G.; Simons, L. H.; van Schijndel, J. W.; Barnett, P.; Balzar, M.; Dekker, H.; van der Linden, C.; Wever, R. *Biochem. Soc. Trans.* **1995**, *23*, 267. (b) Butler, A. *Coord. Chem. Rev.* **1999**, *187*, 17. (c) Wever, R. In *Vanadium: Biochemical and Molecular Biological Approaches*; Michibata, H., Ed.; Springer Science+Business Media B.: New York, 2012; pp 95−125.

(2) (a) Van Schijndel, J. W.; Barnett, P.; Roelse, J.; Vollenbroek, E. G.; Wever, R. *Eur. J. Biochem.* **1994**, *225*, 151. (b) Macedo-Ribeiro, S.; Hemrika, W.; Renirie, R.; Wever, R.; Messerschmidt, A. *J. Biol. Inorg. Chem.* **1999**, *4*, 209. (c) Wever, R.; van der Horst, M. A. *Dalton Trans.* **2013**, *42*, 11778.

(3) (a) van de Velde, F.; van Rantwijk, F.; Sheldon, R. A. *Trends Biotechnol.* **2001**, *19*, 73. (b) Dembitsky, V. M. *Tetrahedron* **2003**, *59*, 4701.

(4) Pooransingh, N.; Pomerantseva, E.; Ebel, M.; Jantzen, S.; Rehder, D.; Polenova, T. *Inorg. Chem.* **2003**, *42*, 1256.

(5) Hasan, Z.; Renirie, R.; Kerkman, R.; Ruijssenaars, H. J.; Hartog, A. F.; Wever, R. *J. Biol. Chem.* **2006**, *281*, 9738.

(6) (a) Hemrika, W.; Renirie, R.; Macedo-Ribeiro, S.; Messerschmidt, A.; Wever, R. *J. Biol. Chem.* **1999**, *274*, 23820. (b) Tanaka, N.; Hasan, Z.; Wever, R. *Inorg. Chim. Acta* **2003**, *356*, 288.

(7) (a) Messerschmidt, A.; Wever, R. *Proc. Natl. Acad. Sci. U.S.A.* **1996**, *93*, 392. (b) Messerschmidt, A.; Prade, L.; Wever, R. *Biol. Chem.* **1997**, *378*, 309.

(8) Renirie, R.; Charnock, J. M.; Garner, C. D.; Wever, R. *J. Inorg. Biochem.* **2010**, *104*, 657.

(9) (a) Deboer, E.; Boon, K.; Wever, R. *Biochemistry* **1988**, *27*, 1629. (b) Vanschijndel, J. W. P. M.; Vollenbroek, E. G. M.; Wever, R. *Biochim. Biophys. Acta* **1993**, *1161*, 249.

(10) Battistuzzi, G.; Bellei, M.; Bortolotti, C. A.; Sola, M. *Arch. Biochem. Biophys.* **2010**, *500*, 21.

(11) (a) Renirie, R.; Hemrika, W.; Wever, R. *J. Biol. Chem.* **2000**, *275*, 11650. (b) Renirie, R.; Hemrika, W.; Piersma, S. R.; Wever, R. *Biochemistry* **2000**, *39*, 1133.

(12) Pooransingh-Margolis, N. Ph.D. Thesis, University of Delaware, Newark, DE, 2006.

(13) Rehder, D.; Polenova, T.; Bühl, M. *Annu. Rep. NMR Spectrosc.* **2007**, *62*, 49.

DOI: 10.1021/jacs.5b02635
J. Am. Chem. Soc. 2015, 137, 5618−5628

(14) (a) Skibsted, J.; Jacobsen, C. J. H.; Jakobsen, H. J. *Inorg. Chem.* **1998**, *37*, 3083. (b) Nielsen, U. G.; Jakobsen, H. J.; Skibsted, J. *Inorg. Chem.* **2000**, *39*, 2135. (c) Nielsen, U. G.; Jakobsen, H. J.; Skibsted, J. *J. Phys. Chem. B* **2001**, *105*, 420. (d) Ooms, K. J.; Bolte, S. E.; Smee, J. J.; Baruah, B.; Crans, D. C.; Polenova, T. *Inorg. Chem.* **2007**, *46*, 9285. (e) Nica, S.; Buchholz, A.; Rudolph, M.; Schweitzer, A.; Wächtler, M.; Breitzke, H.; Buntkowsky, G.; Plass, W. *Eur. J. Inorg. Chem.* **2008**, *2008*, 2350. (f) Bolte, S. E.; Ooms, K. J.; Polenova, T.; Baruah, B.; Crans, D. C.; Smee, J. J. *J. Chem. Phys.* **2008**, *128*, 052317. (g) Schweitzer, A.; Gutmann, T.; Wächtler, M.; Breitzke, H.; Buchholz, A.; Plass, W.; Buntkowsky, G. *Solid State Nucl. Magn. Reson.* **2008**, *34*, 52. (h) Ooms, K. J.; Bolte, S. E.; Baruah, B.; Choudhary, M. A.; Crans, D. C.; Polenova, T. *Dalton Trans.* **2009**, 3262. (i) Smee, J. J.; Epps, J. A.; Ooms, K.; Bolte, S. E.; Polenova, T.; Baruah, B.; Yang, L. Q.; Ding, W. J.; Li, M.; Willsky, G. R.; la Cour, A.; Anderson, O. P.; Crans, D. C. *J. Inorg. Biochem.* **2009**, *103*, 575. (j) Fenn, A.; Wächtler, M.; Gutmann, T.; Breitzke, H.; Buchholz, A.; Lippold, I.; Plass, W.; Buntkowsky, G. *Solid State Nucl. Magn. Reson.* **2009**, *36*, 192. (k) Chatterjee, P. B.; Goncharov-Zapata, O.; Quinn, L. L.; Hou, G.; Hamaed, H.; Schurko, R. W.; Polenova, T.; Crans, D. C. *Inorg. Chem.* **2011**, *50*, 9794. (l) Goncharova-Zapata, O.; Chatterjee, P. B.; Hou, G.; Quinn, L. L.; Li, M.; Yehl, J.; Crans, D. C.; Polenova, T. *CrystEngComm* **2013**, *15*, 8776.

(15) Gutmann, T.; Schweitzer, A.; Wachtler, M.; Breitzke, H.; Blichholz, A.; Plass, W.; Buntkowsky, G. *Z. Phys. Chem.* **2008**, *222*, 1389.

(16) (a) Elena, B.; Pintacuda, G.; Mifsud, N.; Emsley, L. *J. Am. Chem. Soc.* **2006**, *128*, 9555. (b) *NMR Crystallography*; Harris, R. K., Wasylishen, R. E., Duer, M. J., Eds.; John Wiley & Sons Ltd.: Chichester, UK, 2009; p 520. (c) Widdifield, C. M.; Bryce, D. L. *Phys. Chem. Chem. Phys.* **2009**, *11*, 7120. (d) Lai, J.; Niks, D.; Wang, Y.; Domratcheva, T.; Barends, T. R.; Schwarz, F.; Olsen, R. A.; Elliott, D. W.; Fatmi, M. Q.; Chang, C. E.; Schlichting, I.; Dunn, M. F.; Mueller, L. J. *J. Am. Chem. Soc.* **2011**, *133*, 4. (e) Reinholdt, M.; Croissant, J.; Di Carlo, L.; Granier, D.; Gaveau, P.; Bégu, S.; Devoisselle, J. M.; Mutin, P. H.; Smith, M. E.; Bonhomme, C.; Gervais, C.; van der Lee, A.; Laurencin, D. *Inorg. Chem.* **2011**, *50*, 7802. (f) Martineau, C.; Cadiau, A.; Bouchevreau, B.; Senker, J.; Taulelle, F.; Adil, K. *Dalton Trans* **2012**, *41*, 6232. (g) Baias, M.; Dumez, J. N.; Svensson, P. H.; Schantz, S.; Day, G. M.; Emsley, L. *J. Am. Chem. Soc.* **2013**, *135*, 17501. (h) Perras, F. A.; Korobkova, I.; Bryce, D. L. *CrystEngComm* **2013**, *15*, 8727. (i) Martineau, C. *Solid State Nucl. Magn. Reson.* **2014**, *63*−*64*, 1. (j) Davies, E.; Muller, K. H.; Wong, W. C.; Pickard, C. J.; Reid, D. G.; Skepper, J. N.; Duer, M. J. *Proc. Natl. Acad. Sci. U.S.A.* **2014**, *111*, E1354. (k) Hildebrand, M.; Hamaed, H.; Namespetra, A. M.; Donohue, J. M.; Fu, R.; Hung, I.; Gan, Z.; Schurko, R. W. *CrystEngComm* **2014**, *16*, 7334.

(17) Li, M.; Yehl, J.; Hou, G.; Chatterjee, P. B.; Goldbourt, A.; Crans, D. C.; Polenova, T. *Inorg. Chem.* **2015**, *54*, 1363.

(18) (a) Pooransingh-Margolis, N.; Renirie, R.; Hasan, Z.; Wever, R.; Vega, A. J.; Polenova, T. *J. Am. Chem. Soc.* **2006**, *128*, 5190. (b) Polenova, T.; Pooransingh-Margolis, N.; Rehder, D.; Renirie, R.; Wever, R. In *Vanadium: The Verastile Metal*; Kustin, K., Pessoa, J. C., Crans, D. C., Eds.; Oxford University Press: New York, 2007; Vol. *974*, pp 178−202.

(19) (a) Zampella, G.; Kravitz, J. Y.; Webster, C. E.; Fantucci, P.; Hall, M. B.; Carlson, H. A.; Pecoraro, V. L.; De Luca, L. *Inorg. Chem.* **2004**, *43*, 4127. (b) Kravitz, J. Y.; Pecoraro, V. L.; Carlson, H. A. *J. Chem. Theory Comput.* **2005**, *1*, 1265. (c) Waller, M. P.; Bühl, M.; Geethalakshmi, K. R.; Wang, D.; Thiel, W. *Chem.—Eur. J.* **2007**, *13*, 4723.

(20) Wever, R.; Hemrika, W. In *Vanadium Haloperoxidases*; Messerschmidt, A., Huber, R., Poulos, T., Wieghardt, K., Eds.; John Wiley & Sons, Ltd.: Chichester, 2001.

(21) Bak, M.; Rasmussen, J. T.; Nielsen, N. C. *J. Magn. Reson.* **2000**, *147*, 296.

(22) (a) Haeberlen, U. In *Advances in Magnetic Resonance, Suppl. 1*; Waugh, J. S., Ed.; Academic Press: New York/London, 1976. (b) Spiess, H. W. In *NMR Basic Principles and Progress*; Diehl, P., Fluck, E., Kosfeld, R., Eds.; Spinger-Verlag: Berlin, 1978; Vol. *15*. (c) Mehring, M. *Principles of High Resolution NMR in Solids*; Spinger-Verlag: New York, 1983.

(23) Frisch, M. J.; Trucks, G. W.; Schlegel, H. B.; Scuseria, G. E.; Robb, M. A.; Cheeseman, J. R.; Scalmani, G.; Barone, V.; Mennucci, B.; Petersson, G. A.; Nakatsuji, H.; Caricato, M.; Li, X.; Hratchian, H. P.; Izmaylov, A. F.; Bloino, J.; Zheng, G.; Sonnenberg, J. L.; Hada, M.; Ehara, M.; Toyota, K.; Fukuda, R.; Hasegawa, J.; Ishida, M.; Nakajima, T.; Honda, Y.; Kitao, O.; Nakai, H.; Vreven, T.; Montgomery, J. A., Jr.; Peralta, J. E.; Ogliaro, F.; Bearpark, M.; Heyd, J. J.; Brothers, E.; Kudin, K. N.; Staroverov, V. N.; Kobayashi, R.; Normand, J.; Raghavachari, K.; Rendell, A.; Burant, J. C.; Iyengar, S. S.; Tomasi, J.; Cossi, M.; Rega, N.; Millam, M. J.; Klene, M.; Knox, J. E.; Cross, J. B.; Bakken, V.; Adamo, C.; Jaramillo, J.; Gomperts, R.; Stratmann, R. E.; Yazyev, O.; Austin, A. J.; Cammi, R.; Pomelli, C.; Ochterski, J. W.; Martin, R. L.; Morokuma, K.; Zakrzewski, V. G.; Voth, G. A.; Salvador, P.; Dannenberg, J. J.; Dapprich, S.; Daniels, A. D.; Farkas, Ö.; Foresman, J. B.; Ortiz, J. V.; Cioslowski, J.; Fox, D. J. *Gaussian 09*, revision D.01; Gaussian, Inc.: Wallingford, CT, 2009.

(24) (a) Hou, G.; Yan, S.; Sun, S.; Han, Y.; Byeon, I. J.; Ahn, J.; Concel, J.; Samoson, A.; Gronenborn, A. M.; Polenova, T. *J. Am. Chem. Soc.* **2011**, *133*, 3943. (b) Hou, G.; Byeon, I. J.; Ahn, J.; Gronenborn, A. M.; Polenova, T. *J. Am. Chem. Soc.* **2011**, *133*, 18646. (c) Sun, S.; Yan, S.; Guo, C.; Li, M.; Hoch, J. C.; Williams, J. C.; Polenova, T. *J. Phys. Chem. B* **2012**, *116*, 13585. (d) Hou, G.; Yan, S.; Trébosc, J.; Amoureux, J. P.; Polenova, T. *J. Magn. Reson.* **2013**, *232*, 18. (e) Hou, G.; Lu, X.; Vega, A. J.; Polenova, T. *J. Chem. Phys.* **2014**, *141*, 104202.

(25) (a) Hoult, D. I.; Richards, R. E. *J. Magn. Reson.* **1976**, *24*, 71. (b) Zilm, K. W. The 53rd Experimental Nuclear Magnetic Resonance Conference (ENC), Miami, FL, 2012.

(26) Doty, F. D. In *Encyclopedia of NMR*; Harris, R. K., Wasylishen, R. E., Eds.; John Wiley & Sons, Ltd.: New York, 2012; Vol. *6*, pp 3540−3551.

(27) Nieuwkoop, A. J.; Franks, W. T.; Rehbein, K.; Diehl, A.; Akbey, Ü.; Engelke, F.; Emsley, L.; Pintacuda, G.; Oschkinat, H. *J. Biomol. NMR* **2015**, *61*, 161.

(28) (a) Butler, A.; Eckert, H. *J. Am. Chem. Soc.* **1989**, *111*, 2802. (b) Rehder, D.; Casny, M.; Grosse, R. *Magn. Reson. Chem.* **2004**, *42*, 745.

(29) (a) Bangesh, M.; Plass, W. *J. Mol. Struct. (THEOCHEM)* **2005**, *725*, 163. (b) Raugei, S.; Carloni, P. *J. Phys. Chem. B* **2006**, *110*, 3747.

(30) Zhang, Y.; Gascón, J. A. *J. Inorg. Biochem.* **2008**, *102*, 1684.

(31) Zampella, G.; Fantucci, P.; Pecoraro, V. L.; De Gioia, L. *Inorg. Chem.* **2006**, *45*, 7133.

(32) Zampella, G.; Fantucci, P.; Pecoraro, V. L.; De Gioia, L. *J. Am. Chem. Soc.* **2005**, *127*, 953.

DOI: 10.1021/jacs.5b02635
J. Am. Chem. Soc. 2015, 137, 5618−5628